PROCEEDINGS A

rspa.royalsocietypublishing.org

Research

Cite this article: Duley JM, Fowler AC, Moyles IR, O'Brien SBG. 2017 On the Keller–Rubinow model for Liesegang ring formation. *Proc. R. Soc. A* **473**: 20170128.
http://dx.doi.org/10.1098/rspa.2017.0128

Received: 20 February 2017
Accepted: 21 August 2017

Subject Areas:
physical chemistry, mathematical modelling

Keywords:
Liesegang rings, Keller–Rubinow model, supersaturation theory

Author for correspondence:
A. C. Fowler
e-mail: andrew.fowler@ul.ie

This paper is dedicated with fondness and sadness to the memory of Joe Keller.

THE ROYAL SOCIETY PUBLISHING

On the Keller–Rubinow model for Liesegang ring formation

J. M. Duley[1], A. C. Fowler[1,2], I. R. Moyles[1] and S. B. G. O'Brien[1]

[1]MACSI, University of Limerick, Limerick, Republic of Ireland
[2]OCIAM, University of Oxford, Oxford, UK

ACF, 0000-0002-2062-6372

We study the model of Keller & Rubinow (Keller & Rubinow 1981 *J. Chem. Phys* **74**, 5000–5007. (doi: 10.1063/1.441752)) describing the formation of Liesegang rings due to Ostwald's supersaturation mechanism. Keller and Rubinow provided an approximate solution both for the growth and equilibration of the first band, and also for the formation of secondary bands, based on a presumed asymptotic limit. However, they did not provide a parametric basis for the assumptions in their solution, nor did they provide any numerical corroboration, particularly of the secondary band formation. Here, we provide a different asymptotic solution, based on a specific parametric limit, and we show that the growth and subsequent cessation of the first band can be explained. We also show that the model is unable to explain the formation of finite width secondary bands, and we confirm this result by numerical computation. We conclude that the model is not fully posed, lacking a transition variable which can describe the hysteretic switch across the nucleation threshold.

1. Introduction

Liesegang rings are a series of banded precipitates which form in a number of chemical reactions. Their name is associated with their discovery by Liesegang [1], who described them in the context of the precipitation of silver dichromate as a consequence of the reaction of silver nitrate with potassium dichromate:

$$2AgNO_3 + K_2Cr_2O_7 \rightarrow Ag_2Cr_2O_7 + 2KNO_3. \quad (1.1)$$

A typical experimental situation is shown in figure 1. A gel is formed of a weak solution of potassium dichromate, and a thin layer of silver nitrate is then put on the surface. Over a period of a few days, a series of bands is formed as shown. If the gel is

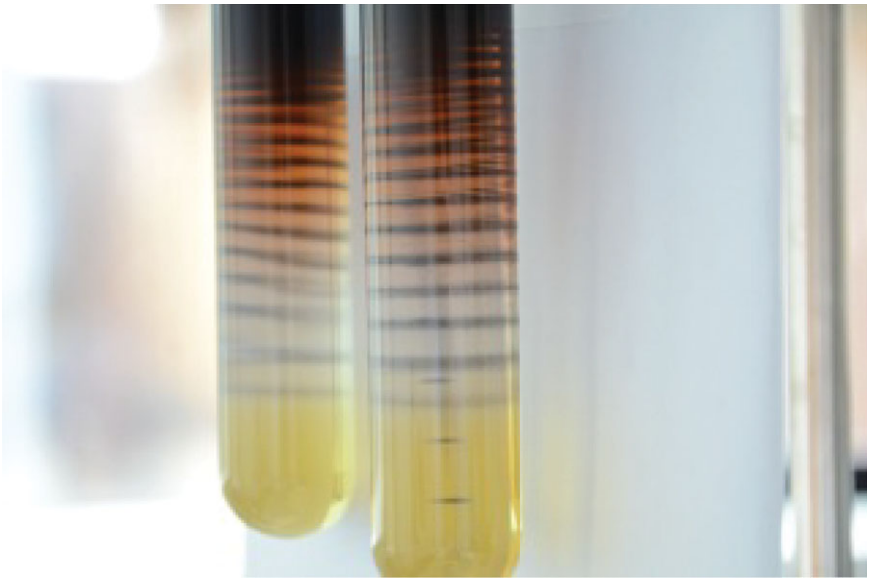

Figure 1. Formation of Liesegang bands in test tubes. Image courtesy of Richard Katz. (Online version in colour.)

placed in a Petri dish, with a drop of silver nitrate at the centre, a series of concentric rings is formed.

The basic mechanism for the formation of the bands was identified by Ostwald [2,3], and studied by a number of early workers, among them Morse & Peirce [4], Wagner [5] and Prager [6]; a useful survey of some of this historical work is given in the short book by Henisch [7]. There are a number of scaling laws which have been found to apply in these experiments. The 'spacing law' was described by Jablczynski [8]: if x_n marks the distance of formation of the nth band from the initial interface of the dichromate with the silver nitrate, then the ratio x_{n+1}/x_n is a constant; normally, greater than one as in figure 1, but occasionally less than one (the so-called revert patterning). Second, there is the 'time law' [4], which states that $x_n \propto \sqrt{t}$, indicating the diffusional nature of the phenomenon. There is also a width law, which states that the successive band widths w_n also form a geometric progression, although it seems this is less reliable than the other two laws.

Early theories of Liesegang patterning are described by Stern [9], who concluded that Ostwald's supersaturation theory appeared adequate for most purposes. In particular, the space and time laws indicate a self-similarity due to the diffusive nature of the dynamics, and these form the basis of the discussions of Prager [6] and Wagner [5]. However, it is not until the paper of Keller & Rubinow [10] that a more sophisticated degree of modelling and analysis was applied. As do their predecessors, Keller and Rubinow describe the reaction (1.1) as the schematic

$$2\mathrm{A} + \mathrm{B} \underset{k_-}{\overset{k_+}{\rightleftharpoons}} \mathrm{C} \xrightarrow{p} \mathrm{D}, \tag{1.2}$$

in which A denotes Ag^+, B denotes $Cr_2O_7^{2-}$, C denotes $Ag_2Cr_2O_7^{\mathrm{L}}$ (i.e. dissolved) and D denotes $Ag_2Cr_2O_7^{\mathrm{S}}$ (i.e. precipitated). Various forms of the theory which is then developed are distinguished, depending on what is assumed about the precipitation rate p. Keller and Rubinow adopt the simple assumption concerning supersaturated nucleation:

$$p = \begin{cases} q[c - c_{\mathrm{s}}]_+ & \text{if } c \geq c_{\mathrm{n}} > c_{\mathrm{s}} \text{ or } d > 0, \\ 0 & \text{if } c < c_{\mathrm{n}} \text{ and } d = 0, \end{cases} \tag{1.3}$$

where $[x]_+ = \max(x, 0)$, c_s is the saturation concentration of C and c_n is the required supersaturation for nucleation: d is the concentration of D, all of these being measured in moles l^{-1} (M). Equation (1.3) states that if no crystal is present, then nucleation and subsequent crystal growth does not commence until the concentration c reaches the supersaturated value c_n, whereas once a crystal is present, it continues to grow for any concentration above the saturation value c_s.

A different version of the theory is called 'post-nucleation theory' (e.g. [11,12]), and is based on a number of experimental results [13], such as those of Kai *et al*. [14], who inferred that nucleation occurred homogeneously in space, but that then precipitation bands formed through the process of Ostwald ripening, in which larger particles grow at the expense of smaller ones. A particular experiment of note in this context is that of Volford *et al*. [15]. In this case, one can posit a precipitation rate given by Mimura *et al*. [16], Venzl & Ross [17] and Falkowitz & Keller [18]

$$\left.\begin{aligned} p &= 4\pi q R^2 R_t \\ \text{and} \qquad RR_t &= k(c - c_a), \end{aligned}\right\} \tag{1.4}$$

where R is the mean crystal radius, a subscript t denotes a partial time derivative and c_a is given in terms of the Gibbs–Thomson relation by

$$c_a = \frac{G}{R}, \quad G = \frac{2\gamma T_M}{\rho_s m_L L}, \tag{1.5}$$

where γ is surface energy, T_M is (crystallization) temperature, ρ_s is crystal density, m_L is the liquidus slope and L is the latent heat. More generally, there is a distribution of grain sizes described by nucleation/growth kinetics [19]. For smaller particles, c_a is larger, and thus R_t and thus also R is smaller, and in fact (1.4) indicates bistability, with either $R \to 0$ or complete solid crystal precipitation being indicated.

There have been a number of models developed, either for the Ostwald supersaturation mechanism, or for various versions of the post-nucleation theory [20,21]. In particular, many such simulations have been produced by Lagzi and co-workers [22–24]. Although all the various models are based around the same basic reaction and precipitation, their implementation varies as to whether Ostwald supersaturation or Ostwald ripening is considered, and in either case short wave stabilization may be included through a Cahn–Hilliard fourth derivative term [18,24].

Our purpose here is somewhat orthogonal to the direction the subject has gone in recent years. Keller & Rubinow [10] proposed a partial analytic solution of the reaction–diffusion supersaturation model, but the basis of this solution was not followed through, or even validated. Our purpose here is to attempt to throw some analytic understanding on the problem, but we are less concerned with the fundamental distinction between the supersaturation and the post-nucleation models. While Ross and co-workers (e.g. [11,13]) have emphasized the distinction between these two theories, they do not appear so dissimilar as mathematical models.

Our initial investigations sought to establish the basis of the Keller–Rubinow approximations, but we have gone far beyond such a limited aspiration. Firstly, we cannot find any régime in which the Keller–Rubinow theory is asymptotically valid. Worse, we believe that the model as stated is actually not well-posed, in a sense which we will explain. In so doing, we resolve, apparently for the first time, the nature of this ill-posedness and its consequent implication for numerical solutions, and we suggest a resolution of the ill-posedness, whose efficacy will be investigated in a future paper.

2. Nucleation and crystal growth

An immediate difficulty with the Keller/Rubinow precipitation rate (1.3) is that p is a discontinuous function at $d = 0$, and numerical solutions of the model have a proclivity to produce Liesegang 'bands' which are one grid point wide (this point will be elaborated in §5). There is thus the suspicion that the model (1.3) is overly simplified and results in ill-posedness. Additionally, there is very little to guide what appropriate choices of the parameters are. We therefore study the issue of nucleation and crystal growth a little more carefully.

A common discussion of nucleation concerns homogeneous nucleation, where the surface energy of the crystal interface provides an energy barrier to nucleation (e.g. [25]); in order to provide a deterministic mechanism to overcome this, a stochastic theory such as Becker–Döring theory is necessary [26,27]. However in practice, nucleation occurs heterogeneously, on pre-existing impurities in the liquid. To understand how this occurs, consider an area A of a solid impurity in contact with a liquid solution, where the chemical potential of the liquid is μ^{L}. We suppose that the chemical potential of the solid precipitate is μ^{S}, and the two are related, for a dilute solution, by

$$\Delta\mu = \mu^{\mathrm{L}} - \mu^{\mathrm{S}} = kT \ln\left(\frac{c}{c_{\mathrm{s}}}\right), \tag{2.1}$$

where c_{s} is the saturation concentration in the liquid, k is Boltzmann's constant and T is the absolute temperature. (Thus, when $c = c_{\mathrm{s}}$, the solid and liquid are in equilibrium.) If the area forms a nucleus of precipitate consisting of N molecules with chemical potential μ^{S}, then the change in free energy is $-(\mu^{\mathrm{L}} - \mu^{\mathrm{S}})N = -N\Delta\mu$, but the corresponding change of surface energy is $A\Delta\gamma$, where

$$\Delta\gamma = \gamma_{\mathrm{SI}} + \gamma_{\mathrm{SL}} - \gamma_{\mathrm{LI}}, \tag{2.2}$$

and γ_{jk} is the surface energy at the interface between phase j and phase k (S, L, I indicate solid, liquid, impurity, respectively). If the nucleated solid phase is (initially) a monolayer, then $N = A/d_{\mathrm{m}}^2$, where d_{m} is the molecular diameter, and thus the total free energy change is

$$\Delta G = \left(\Delta\gamma - \frac{\Delta\mu}{d_{\mathrm{m}}^2}\right) A. \tag{2.3}$$

We thus see that heterogeneous nucleation occurs 'spontaneously' if

$$\Delta\mu > \Delta\mu_{\mathrm{c}} = d_{\mathrm{m}}^2 \Delta\gamma, \tag{2.4}$$

and for dilute solutions, this gives an estimate of the nucleation threshold c_{n} as

$$c_{\mathrm{n}} - c_{\mathrm{s}} \approx \frac{d_{\mathrm{m}}^2 c_{\mathrm{s}} \Delta\gamma}{kT}. \tag{2.5}$$

This assumes that the growth process on the impurity forms an approximate monolayer rather than growing a local cap; this depends on the kinetics of growth on the surface.

(a) Growth rate

Next we may ask what the growth rate is, once nucleation has occurred. This is provided by Lifshitz–Slyozov theory [28]. The idea is that a spherical crystal sits in a solution which is supersaturated in the far field, but at (unstable) equilibrium (where the free energy is a maximum) at the interface, and the resultant diffusion of the solute to the interface provides the growth rate.

The free energy change associated with the presence of the crystal is not simply that given by (2.3), because of the finite volume of the precipitate. More precisely, suppose that a spherical impurity of diameter d_{I} has a layer of precipitate on it, such that the total crystal diameter is d_{c}. It follows that the change of free energy from the original state is

$$\Delta G = \pi[\gamma_{\mathrm{SL}} d_{\mathrm{c}}^2 + \gamma_{\mathrm{SI}} d_{\mathrm{I}}^2 - \gamma_{\mathrm{LI}} d_{\mathrm{I}}^2] - \frac{\pi\Delta\mu}{6v_{\mathrm{m}}}(d_{\mathrm{c}}^3 - d_{\mathrm{I}}^3), \tag{2.6}$$

where $v_{\mathrm{m}} = \frac{1}{6}\pi d_{\mathrm{m}}^3$ is the molecular volume. Using (2.2), we can write this in the form

$$\Delta G = \pi d_{\mathrm{I}}^2 \left[\Delta\gamma + \gamma_{\mathrm{SL}}\left\{\left(\frac{d_{\mathrm{c}}}{d_{\mathrm{I}}}\right)^2 - 1\right\}\right] - \frac{d_{\mathrm{I}}^3 \Delta\mu}{d_{\mathrm{m}}^3}\left[\left(\frac{d_{\mathrm{c}}}{d_{\mathrm{I}}}\right)^3 - 1\right]. \tag{2.7}$$

This expression mimics the situation for homogeneous nucleation, where, for small d_{c}, the surface energy causes an initial increase $\pi d_{\mathrm{I}}^2 \Delta\gamma$ of ΔG, thus forming a barrier to nucleation. This discontinuity is due to the replacement of a single impurity/solution interface with a pair of interfaces, solution/precipitate and precipitate/impurity.

This seems to contradict (2.4). In more detail, we calculate, from (2.7),

$$\frac{\partial \Delta G}{\partial d_c} = \frac{3 d_c \Delta\gamma}{d_m}\left[\frac{2\pi}{3}\frac{\gamma_{SL}}{\Delta\gamma} d_m - \left(\frac{\Delta\mu}{\Delta\mu_c}\right) d_c\right], \tag{2.8}$$

which gives a threshold crystal size for growth (when ΔG is a maximum, i.e. when the right-hand side of (2.8) is zero). However, we may note that, on the basis that $d_m \ll d_I \approx d_c$, the first term in square brackets is negligible compared to the second, and can be ignored. This then raises a further issue, which is that apparently (2.8) would imply that the condition for heterogeneous nucleation is simply $\Delta\mu > 0$, as opposed to (2.4). The resolution of this is to note that the discontinuity of ΔG given by (2.7) at $d_c = d_I$ is in reality smoothed out by the supposition that the surface energy varies continuously as the precipitate layer thickness increases, thus

$$\Delta G = \pi d_I^2\left[\phi(h)\Delta\gamma + \gamma_{SL}\left\{\left(\frac{d_c}{d_I}\right)^2 - 1\right\}\right] - \frac{d_I^3 \Delta\mu}{d_m^3}\left[\left(\frac{d_c}{d_I}\right)^3 - 1\right], \tag{2.9}$$

where $\phi(h)$ is a dimensionless function of layer thickness $h = d_c - d_I$ which varies from $\phi(0) = 0$ to $\phi(\infty) = 1$ over a length scale $h \sim d_m$; in particular, $d_m\phi'(0) \sim O(1)$. The function ϕ makes ΔG continuous, and is due to short-range intermolecular forces similar to those which determine disjoining pressure [29]. Ignoring the small term in γ_{SL}, (2.8) is modified, for $h \sim d_m$, to

$$\frac{\partial \Delta G}{\partial d_c} = \frac{3 d_c^2 \Delta\gamma}{d_m}\left[\frac{\pi d_m \phi'}{3} - \frac{\Delta\mu}{\Delta\mu_c}\right], \tag{2.10}$$

and as $d_m\phi'(0) \sim O(1)$, (2.4) is regained, depending on the precise value of $\phi'(0)$.

The upshot of this is that once the precipitate layer is sufficiently thick (many molecular diameters), we can take $\Delta\mu = 0$, thus $c = c_s$, at the interface, and the resultant growth rate is obtained by solving the (steady-state) diffusion equation and equating the resulting flux at the surface to the crystal growth rate [28], which leads to

$$\dot{d}_c = \frac{4 D V_c (c - c_s)}{d_c}, \tag{2.11}$$

where D is the diffusion coefficient of the solute and V_c is the molar volume of the precipitate (equal to its molecular weight divided by the density). To convert this to a growth rate p in (1.3), where we suppose that the units of concentration are moles l^{-1} (M), and thus the units of p are moles l^{-1} s^{-1} (the units of q are s^{-1}), we note that the precipitate concentration is

$$d = \frac{\pi n_I (d_c^3 - d_I^3)}{6 V_c}, \tag{2.12}$$

where n_I is the number of impurities per litre (the impurities are assumed to be of the same size). Relating this to (1.3), we find that the Keller/Rubinow form is justified, and the rate coefficient q is given by

$$q = 2\pi n_I d_I D\left[1 + \frac{V_c d}{V_I}\right]^{1/3}, \tag{2.13}$$

where $V_I = \frac{1}{6}\pi n_I d_I^3$ is the volume density (m^3 l^{-1}) of the impurity. All of this discussion simply reinforces the Keller/Rubinow assumption in (1.3) of a discontinuous growth rate.

3. Mathematical model

In order to focus attention, we begin with a statement of the Keller–Rubinow model. The reaction scheme we consider is that given in (1.2), for which the relevant equations are, assuming a one-dimensional domain,

$$\left.\begin{aligned} a_t &= D_A a_{xx} - 2r, \\ b_t &= D_B b_{xx} - r, \\ c_t &= D_C c_{xx} + r - p \end{aligned}\right\} \quad \text{and} \quad d_t = p, \tag{3.1}$$

where r is the reaction rate, given by

$$r = k_+ a^2 b - k_- c, \tag{3.2}$$

and the small letters indicate the concentrations of the corresponding chemical species: a represents silver and b dichromate. The precipitation rate is given by (1.3):

$$p = \begin{cases} q[c - c_\mathrm{s}]_+ & \text{if } c \geq c_\mathrm{n} > c_\mathrm{s} \text{ or } d > 0, \\ 0 & \text{if } c < c_\mathrm{n} \text{ and } d = 0. \end{cases} \tag{3.3}$$

A more sophisticated version of this model is given by Fiałkowski *et al*. [30]. We suppose an initially uniform solution of $b = b_0$ with $a = 0$, and we impose a boundary condition $a = a_0$ at $x = 0$; these correspond to the experimentally imposed conditions.

A comment should be made concerning the choice of the reaction rate r, as it relates to a trimolecular reaction (1.2), or more specifically

$$2\mathrm{Ag}^+ + \mathrm{Cr_2O_7^{2-}} \to \mathrm{Ag_2Cr_2O_7}. \tag{3.4}$$

In principle, this total reaction must be a combination of (at least) two bimolecular steps such as

$$\left.\begin{aligned} \mathrm{A} + \mathrm{B} &\underset{k_{-1}}{\overset{k_1}{\rightleftharpoons}} \mathrm{I} \\ \mathrm{A} + \mathrm{I} &\underset{k_{-2}}{\overset{k_2}{\rightleftharpoons}} \mathrm{C}, \end{aligned}\right\} \quad \text{and} \tag{3.5}$$

where $\mathrm{I} = \mathrm{AgCr_2O_7^-}$, for example. If we then assume that the first of these reactions is very fast and thus in quasi-equilibrium, we regain (3.2), with $k_+ = k_1 k_2 / k_{-1}$ and $k_- = k_{-2}$. Other assumptions can lead to different rates, however. We follow (3.2) as it is the assumption used by Keller and Rubinow.[1]

We assume $D_B = D_C$, and then non-dimensionalize the equations by writing

$$a \sim a_0, \quad b, d \sim b_0, \quad c \sim c_\mathrm{n}, \quad p, r \sim q c_\mathrm{n}, \quad t \sim \frac{b_0}{q c_\mathrm{n}} \quad \text{and} \quad x \sim \sqrt{\frac{D_A b_0}{q c_\mathrm{n}}}, \tag{3.6}$$

whence the dimensionless model is

$$\left.\begin{aligned} a_t &= a_{xx} - 2\varepsilon r, \\ b_t &= \delta b_{xx} - r, \\ \nu c_t &= \nu\delta c_{xx} - p + r \end{aligned}\right\} \quad \text{and} \quad d_t = p, \tag{3.7}$$

[1]In fact, the detail of the bimolecular steps becomes irrelevant when we later assume that the reaction $2\mathrm{A} + \mathrm{B} \rightleftharpoons \mathrm{C}$ is fast.

where

$$p = \begin{cases} [c-\alpha]_+ & \text{if } c \geq 1 \text{ or } d > 0, \\ 0 & \text{if } c < 1 \text{ and } d = 0 \end{cases} \Bigg\} \tag{3.8}$$

and

$$r = \Lambda(\lambda a^2 b - c),$$

and we have defined

$$\alpha = \frac{c_s}{c_n} < 1, \quad \varepsilon = \frac{b_0}{a_0} \ll 1, \quad \nu = \frac{c_n}{b_0}, \quad \delta = \frac{D_B}{D_A}, \quad \lambda = \frac{k_+ a_0^2 b_0}{k_- c_n} \quad \text{and} \quad \Lambda = \frac{k_-}{q}. \tag{3.9}$$

In a saturated solution, we have

$$c = c_s = \frac{k_+ K_{sp}}{k_-}, \tag{3.10}$$

where the solubility product K_{sp} is given by

$$K_{sp} = a_s^2 b_s \tag{3.11}$$

in saturation, and is measured; it follows that

$$\lambda = \frac{\alpha a_0^2 b_0}{a_s^2 b_s}, \tag{3.12}$$

so we can assume $\lambda > \alpha$.

We now paraphrase Keller and Rubinow's development, following Fowler [31, pp. 829 ff.]. Suppose that the reaction is very fast, $\Lambda \gg 1$, so that $r \approx 0$. Then

$$c \approx \lambda a^2 b. \tag{3.13}$$

Suitable initial conditions are

$$a = 0, \quad b = 1, \quad c = d = 0 \quad \text{at} \quad t = 0, \tag{3.14}$$

and suitable boundary conditions are

$$\left.\begin{aligned} &a = 1, \quad b_x = c_x = 0 \quad \text{at } x = 0, \\ \text{and} \quad &a \to 0, \quad b \to 1, \quad c \to 0 \quad \text{as } x \to \infty. \end{aligned}\right\} \tag{3.15}$$

We define the total dichromate

$$B = b + \nu c, \tag{3.16}$$

whence we obtain

$$\left.\begin{aligned} &B_t = \delta B_{xx} - p \\ \text{and} \quad &d_t = p, \end{aligned}\right\} \tag{3.17}$$

and also

$$\left.\begin{aligned} &c = AB, \quad A = \frac{\lambda a^2}{1 + \lambda \nu a^2} \\ \text{and} \quad &p = \begin{cases} [AB - \alpha]_+ & \text{if } AB \geq 1 \text{ or } d > 0, \\ 0 & \text{if } AB < 1 \text{ and } d = 0. \end{cases} \end{aligned}\right\} \tag{3.18}$$

Keller and Rubinow assume that the reaction term r can be neglected in the equation for a because $b_0 \ll a_0$ (the dichromate is very dilute), and it is easy to show this by combining $(3.7)_{1,2}$; thus

$$a = \operatorname{erfc}\left(\frac{x}{2\sqrt{t}}\right). \tag{3.19}$$

The monotonically decreasing function A is thus given by

$$A(\theta) = \frac{\lambda \operatorname{erfc}^2 \theta}{1 + \lambda \nu \operatorname{erfc}^2 \theta}, \quad \theta = \frac{x}{2\sqrt{t}}. \tag{3.20}$$

The initial and boundary conditions are

$$\left.\begin{aligned} B=1, \quad d=0 \quad \text{at } t=0;\\ B_x=0 \quad \text{at } x=0\\ \text{and} \qquad B\to 1 \quad \text{as } x\to\infty. \end{aligned}\right\} \tag{3.21}$$

(a) Primary precipitation

The maximum value of $A=\lambda/(1+\lambda\nu)$ is at $\theta=0$, and thus precipitation occurs at $x=0$ providing $\lambda>1/(1-\nu)$, as we assume (and also $\nu<1$). Keller and Rubinow provide an approximate solution for their model, as follows. Initially, there is a central precipitating region $0<x<s(t)$, where $p>0$, and $p=0$ outside this. As long as $\dot{s}>0$, the concentration must be at the nucleation threshold, thus

$$AB=1 \quad \text{at } x=s, \quad \dot{s}>0. \tag{3.22}$$

Conversely, while s is stationary, we must have

$$AB<1 \quad \text{at } x=s, \quad \dot{s}=0. \tag{3.23}$$

Thus after the front becomes stationary, the possibility of secondary nucleation ahead of the front arises.

Suppose that $A(\theta)$ is slowly varying in space, and that s is slowly varying in time; then a quasi-static solution is appropriate. As B is continuous at s, it follows that $AB=1$ there (if $\dot{s}>0$), and this solution is

$$AB=\alpha+\frac{(1-\alpha)\cosh\left(\sqrt{A^*}x\right)}{\cosh\left(\sqrt{A^*}s\right)}, \tag{3.24}$$

where $A^*=A/\delta$. For $x>s$, a stationary solution is not possible, but for slowly varying s,

$$B=1-\left(1-\frac{1}{A}\right)\operatorname{erfc}\left\{\frac{x-s}{2\sqrt{\delta t}}\right\}. \tag{3.25}$$

Equating the derivatives B_x at $s\pm$, we find that s is determined by the relation

$$\sqrt{A(\Theta)}-\frac{1}{\sqrt{A(\Theta)}}=(1-\alpha)\sqrt{\pi t}\tanh\left(\sqrt{\frac{A(\Theta)}{\delta}}s\right), \tag{3.26}$$

in which $A(\Theta)$ is given by (3.20), but with

$$\Theta=\frac{s}{2\sqrt{t}}. \tag{3.27}$$

To solve this, we define

$$u=\sqrt{\frac{A(\Theta)}{\delta}}s, \tag{3.28}$$

and then (3.26) can be written in the form

$$u\tanh u=\frac{2\Theta}{\sqrt{\delta\pi}}\left\{\frac{A(\Theta)-1}{(1-\alpha)}\right\}. \tag{3.29}$$

The right-hand side is a unimodal (one-humped) function of Θ, while $u\tanh u$ is an increasing function of u. Therefore, $u(\Theta)$ is a positive unimodal function in the range $0<\Theta<\Theta_1$, where $A(\Theta_1)=1$. Consulting (3.26), we see that initially $A=1$ and thereafter increases with t. Therefore, initially $\Theta=\Theta_1$ and decreases with increasing t. As A is increasing as is s, u must increase, but it cannot do so indefinitely, because of the maximum value of $u(\Theta)$. In consequence, there is a finite time t^* when s reaches a maximum s^*, and the solution cannot be continued in this form beyond this time. We then enter a phase where $\dot{s}=0$, and (3.23) applies.

Keller and Rubinow go on to suggest that a sequence of precipitation bands will subsequently form, and they analyse these based on the same approximating solutions. The initial motivation

of our work was to establish the asymptotic basis for their approximation, and then use this to develop the solution explicitly. However, despite a considerable amount of effort, we have not been able to find any asymptotic limit in which the Keller–Rubinow solution holds. Below, we provide an asymptotic description based on the limit $\delta \ll 1$, which bears little resemblance to the Keller–Rubinow theory. The solution has been tested successfully against numerical results, as described in §5.

(b) An asymptotic approximation

We consider the equation (3.17) with $\delta \ll 1$.[2] Specifically, we have

$$\left.\begin{aligned} &B_t = \delta B_{xx} - [AB-\alpha]_+, \quad x<s,\\ &B_t = \delta B_{xx}, \quad x>s,\\ &B_x = 0 \text{ at } x=0, \quad B\to 1 \text{ as } x\to\infty\\ \text{and}\quad &B = \frac{1}{A}, \quad [B_x]^+_- = 0 \text{ at } x=s. \end{aligned}\right\} \tag{3.30}$$

At leading order in δ, the solution is (with an obvious notation for θ' and θ'' and assuming $AB>\alpha$ in $x<s$)

$$\left.\begin{aligned} &B=1, \quad x>s\\ \text{and}\quad &B = \exp\left[-\int_{t_s}^{t} A(\theta')\,\mathrm{d}t'\right] + \alpha\int_{t_s}^{t}\exp\left[-\int_{t'}^{t} A(\theta'')\,\mathrm{d}t''\right]\mathrm{d}t', \quad x<s, \end{aligned}\right\} \tag{3.31}$$

where $t_s(x)$ is the time when the front passes x (because the boundary condition for the equation $B_t=-(AB-\alpha)$ in $x<s$ is $B=1$ at $t=t_s$). The conditions on B_x at $x=0$ and $x=s$ are not satisfied, but are enabled by weak boundary layers there.

It is convenient to write the integrals in terms of $\theta = x/2\sqrt{t}$, noting also that $t=t_s$ at $\theta=\Theta = s/2\sqrt{t}$, where s is determined by the condition

$$A(\Theta)=1; \tag{3.32}$$

thus

$$B = \exp\left[-\frac{1}{2}x^2\int_\theta^\Theta \frac{A(\phi)\,\mathrm{d}\phi}{\phi^3}\right] + \frac{1}{2}\alpha x^2\int_\theta^\Theta \exp\left[-\frac{1}{2}x^2\int_\theta^\phi \frac{A(\psi)\,\mathrm{d}\psi}{\psi^3}\right]\frac{\mathrm{d}\phi}{\phi^3}, \quad x<s. \tag{3.33}$$

Of interest is the slope S of $c=AB$ at $x=s$. This is because we must have $c<1$ in $x>s$, and thus $S<0$. Putting $x=2\sqrt{t}\theta$ and doing the calculation, we find

$$S = \frac{1}{2\sqrt{t}}\left(A' + \frac{2(1-\alpha)t}{\Theta}\right), \tag{3.34}$$

using the fact that $A=B=1$ at $x=s$. As $A'(\Theta)<0$ and Θ are thus fixed, we see that $S<0$ in $x<s$ for $t<t_c$, where

$$t_c = \frac{\Theta_f|A'(\Theta_f)|}{2(1-\alpha)}, \tag{3.35}$$

and $\Theta=\Theta_f$ at $t=t_c$. For $t>t_c$, S in $x<s$ is positive. As $S=A'<0$ in $x>s$, we see that the condition for front advance breaks down at $t=t_c$, and after that the front is stationary. The situation is indicated in figure 2. The subsequent evolution of the solution is considered in §4. Note that (3.34) is apparently only approximate, in view of the weak boundary layer in B; however, analysis of the boundary layer shows that (3.34) remains valid to leading order in δ.[3]

[2]It is also possible to analyse the case $\delta \gg 1$, but this is omitted here, for two reasons: firstly, it is not likely to be physically appropriate, and secondly, it is then generally found that secondary bands do not form.

[3]The boundary layer is analysed by putting $B=1+\delta b$, $x=s+\delta X$, and the result of this leaves (3.34) unaltered. The solution is approximately linear behind the front (the outer solution remains valid), it is exponentially declining ahead of the front, $b=-b_f e^{-\hat{s}(X-X_f)}$, the front shifts to $s=2\Theta\sqrt{t}+\delta X_f$, $X_f\approx -2(1-\alpha)t^{3/2}/\Theta^2|A'(\Theta)|$ and the value of B at the front is $B\approx 1-\delta b_f$, $b_f=(1-\alpha)t/\Theta^2$.

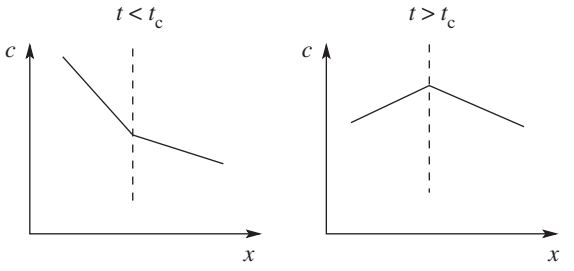

Figure 2. The behaviour of c at the front for (*a*) $t < t_c$ and (*b*) $t > t_c$. The apparent discontinuity in slope at the front is smoothed by a weak boundary layer. The situation in (*b*) is not tenable, and the front stops moving.

4. Secondary banding

We now consider the situation when $t > t_c$. When the primary crystal stops growing,

$$t = t_c, \quad s = s_c = 2\Theta_f\sqrt{t_c}, \tag{4.1}$$

where $A(\Theta_f) = 1$. Subsequent to this, we have to solve

$$\left.\begin{aligned} &B_t = \delta B_{xx} - [AB - \alpha]_+, \quad x < s_c, \\ &B_t = \delta B_{xx}, \quad x > s_c, \\ &B_x = 0 \text{ at } x = 0, \quad B \to 1 \text{ as } x \to \infty, \\ \text{and} \quad &B < \frac{1}{A_c}, \quad [B]^+_- = [B_x]^+_- = 0 \text{ at } x = s, \end{aligned}\right\} \tag{4.2}$$

where $A_c(t) = A(s_c/2\sqrt{t})$. The outer solutions are as before; however, a (strong) boundary layer now develops at $x = s_c$, and can be approximately analysed as follows. We write

$$x = s_c + \sqrt{\delta}X \quad \text{and} \quad t = t_c + \tau, \tag{4.3}$$

and expand $A(\theta)$ near s_c for small τ. The result of this, using (4.1) and (3.35), is

$$A \approx 1 + (1 - \alpha)\tau + \cdots. \tag{4.4}$$

In $X < 0$, we thus have approximately

$$B_\tau = B_{XX} - \{1 + (1 - \alpha)\tau\}B + \alpha. \tag{4.5}$$

The outer solution (ignoring the diffusion term) is just $B \approx 1 - (1 - \alpha)\tau$, and if we define

$$B = 1 - (1 - \alpha)\tau g, \tag{4.6}$$

then to $O(\tau)$, we have (because we can neglect the term $(1 - \alpha)\tau$ in (4.5))

$$g + \tau g_\tau = \tau g_{XX} + 1, \tag{4.7}$$

of which there is a similarity solution for g of the form

$$g = 1 - 4(1 - g_0)\mathrm{i}^2\mathrm{erfc}(-\eta), \quad \eta = \frac{X}{2\sqrt{\tau}}, \tag{4.8}$$

which satisfies the condition $g(-\infty) = 1$, and has $g(0) = g_0$, to be determined.[4]

[4]The error function integral $\mathrm{i}^2\mathrm{erfc}$ is defined in Abramowitz & Stegun [32].

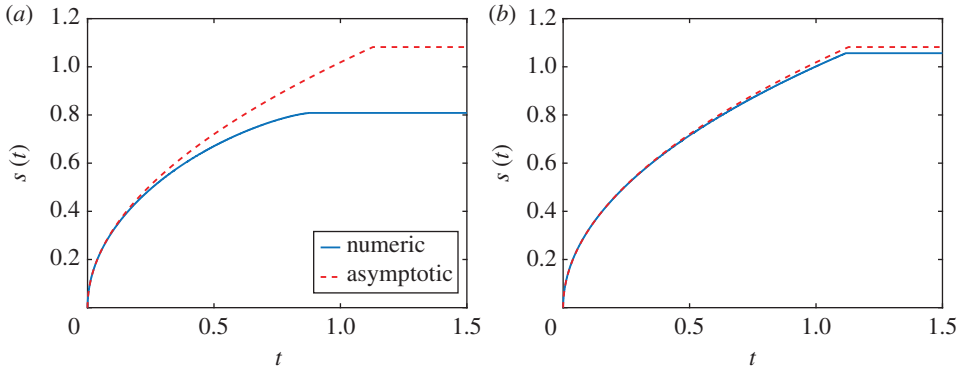

Figure 3. Numerical and asymptotic evolution of the first precipitation front, $s(t)$, for different values of δ. The numerical curve is generated from the solution to (3.17) with parameters $\alpha = 0.25$, $\nu = 0.1$ and $\lambda = 5$. The asymptotic curve is given by $s(t) = 2\Theta\sqrt{t}$ where Θ is given by (3.32). (*a*) $\delta = 0.1$, $t_n = 0.873$, $t_a = 1.129$ and (*b*) $\delta = 0.01$, $t_n = 1.1170$, $t_a = 1.129$. Here t_n and t_a are denoted the numerical and asymptotic times, respectively, where the first precipitation front terminates. (Online version in colour.)

Similarly, in $\eta > 0$, we write

$$B = 1 - (1-\alpha)\tau h(\eta), \quad h = 4g_0 \mathrm{i}^2\mathrm{erfc}\,\eta, \tag{4.9}$$

which satisfies continuity of B at $X = 0$; g_0 is then determined by the condition of continuity of B_X, and this yields $g_0 = \frac{1}{2}$. Combining this with the expansion for A, we find that, in $X > 0$,

$$c = AB \approx 1 + (1-\alpha)\tau\{1 - 2\,\mathrm{i}^2\mathrm{erfc}\,\eta\} + \cdots, \tag{4.10}$$

with a similar expression in $X < 0$. Expanding the repeated error function integral for small η then shows that

$$c \approx 1 + (1-\alpha)\left[\pm\frac{1}{4}X^2 + X\sqrt{\frac{\tau}{\pi}} + \frac{1}{2}\tau\right] + \cdots \quad \text{for } X \lessgtr 0. \tag{4.11}$$

The requirement that $c \leq 1$ at the front is not satisfied, and in addition $c_X > 0$ at the front. As a result, secondary nucleation occurs immediately ahead of the stationary front.

In practice, this situation is untenable, and in numerical computations a series of grid point scale spikes occurs, indicating a failure of the model to proceed past the cessation of the first band. We now describe these results.

5. Numerical results

As we have shown that, under the assumption $\varepsilon \ll 1$, (3.1) reduces to (3.17), we will focus our numerical simulations on the latter system. We simulate (3.17) using a method of lines approach with the stiff ODE solver `ode15s` in MATLAB. We compute a partial Jacobian matrix where we neglect the non-smooth p component and provide this to the solver. We use the numerical results in two ways; firstly, we provide numerical evidence to compare with the asymptotic results obtained concerning the first front; then, we provide numerical results for secondary spike formation.

(a) The first front

Figure 3 shows a comparison of the asymptotic prediction for the front position with the numerical solution at two values of δ. For $\delta = 0.1$, the solution is qualitatively accurate, but for $\delta = 0.01$, it is much more accurate, indicating a consistent asymptotic approach as $\delta \to 0$.

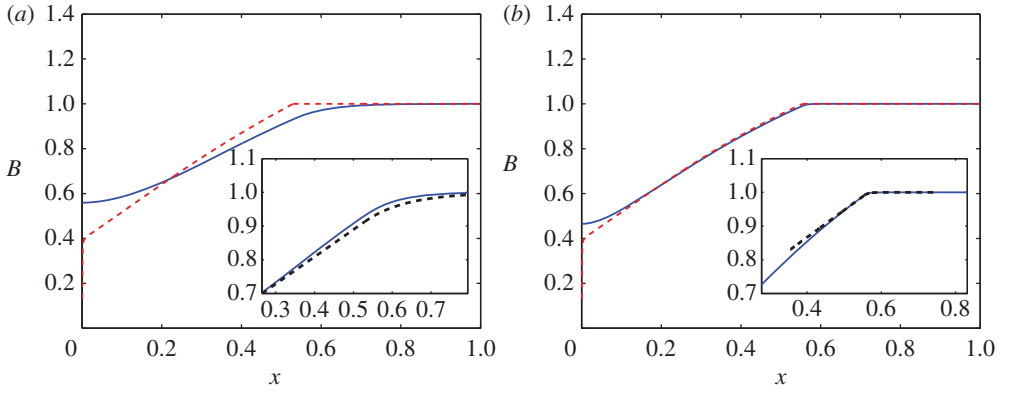

Figure 4. Numerical (solid) and asymptotic (dashed) comparison of $B(x, t)$ for two values of δ at $t = 0.3$ far from when the first front terminates. (*a*) $\delta = 0.1$ and (*b*) $\delta = 0.01$. The numerical solution is generated by solving (3.17) with parameters $\alpha = 0.25$, $\nu = 0.1$ and $\lambda = 5$. The asymptotic solution in the outer figure is given by (3.31), while the inset includes the weak boundary layer near $x = s(t)$ (described in the footnote before the beginning of §4). The boundary layer solution at $x = 0$ has been omitted. (Online version in colour.)

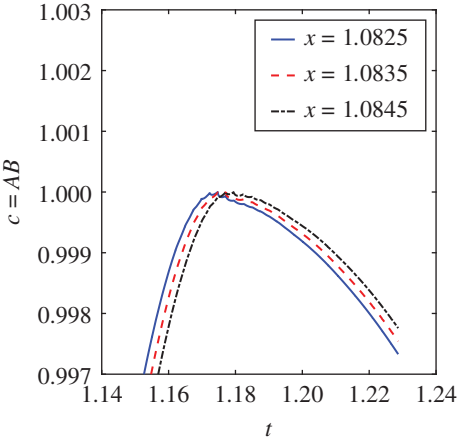

Figure 5. Numerical verification that near $x = s_c$ and $t = t_c$, $c_x > 0$ for $x < s_c$, as shown in figure 2. The numerical solution is computed by solving (3.17) with parameters $\alpha = 0.25$, $\nu = 0.1$, $\lambda = 5$ and $\delta = 0.01$. We see that, for $t < t_c$, $c_x < 0$, while for $t > t_c$, $c_x > 0$, which is consistent with (4.11). (Online version in colour.)

For the same two parameter values, figure 4 shows a comparison of the profile of B, and again the agreement is excellent at the lower δ value. In the inset we include the weak boundary layer at the front referred to in the footnote just before §4, but we have not included that at $x = 0$, which is of less interest.

Finally, in figure 5 we plot the variation of c at three nearby values of x ($x_1 < x_2 < x_3$, say) with time. According to figure 2, for $t < t_c$, c should be monotonically decreasing with x while $x_i < s$, but for $t > t_c$, c becomes monotonically increasing with x. In figure 5, we can see this behaviour, as the ordering of the curves switches at $t \approx 1.17$; equivalently, figure 2 suggests that at fixed x, c should increase with t, reaching $c = 1$ when $x = s$, and thereafter decrease again, and this is clearly the case.

(b) Secondary spikes

In this section, all of our simulations are computed with the parameter set

$$\alpha = 0.25, \quad \nu = 0.1, \quad \lambda = 5 \quad \text{and} \quad \delta = 0.05, \tag{5.1}$$

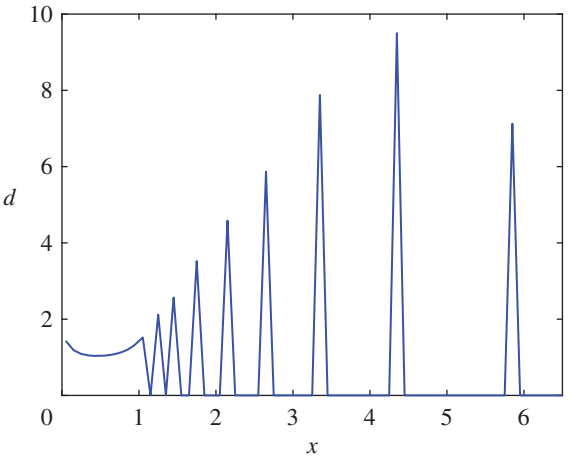

Figure 6. Precipitate d in the numerical solution to (3.17) with a step size of $h = 0.1$ on a grid $[0, 10]$ for $t = 60$. After the first layer terminates growth, secondary spikes emerge with increasing separation. (Online version in colour.)

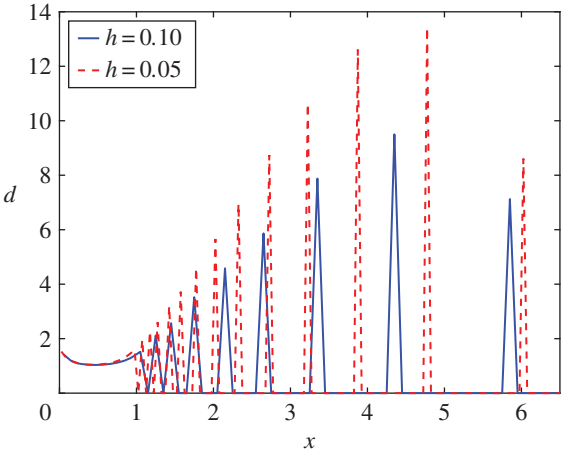

Figure 7. Precipitate d in the numerical solution to (3.17) for two step sizes on a grid $[0, 10]$ for $t = 60$. Refining the step size increases the number of spikes produced and their locations. (Online version in colour.)

where we note that, as $\lambda > 1/(1 - \nu)$, nucleation should commence at $t = 0$. From our analysis, it appears that proper secondary spikes are impossible. As a first example figure 6 shows the final time computation ($t = 60$) of the precipitate d using a grid space of $h = 0.1$ on a domain $[0, 10]$.

At first glance, it appears that secondary spikes form and space out with increasing separation. This type of behaviour has been noted before by people analysing this model [33]. However, this apparent spacing is a numerical artefact, and if we decrease the grid spacing to $h = 0.05$ and recompute the solution, new spikes appear (figure 7). Furthermore, the location of the spikes changes, whereas if the problem was well posed numerically, we would expect a convergent set of solutions to appear for decreasing step size.

The numerical simulations in the literature such as that of Hilhorst *et al*. [33] do not seem to do a numerical refinement study to verify the legitimacy of the spacing they observe. Experimentally, a true spacing law is observed and is due to Jablczynski [8], which states that, for the nth band located at x_n, the ratio x_{n+1}/x_n approaches a constant. We can investigate this numerically by solving (3.17) for various step sizes. Figure 8 shows the predicted space law from solving to

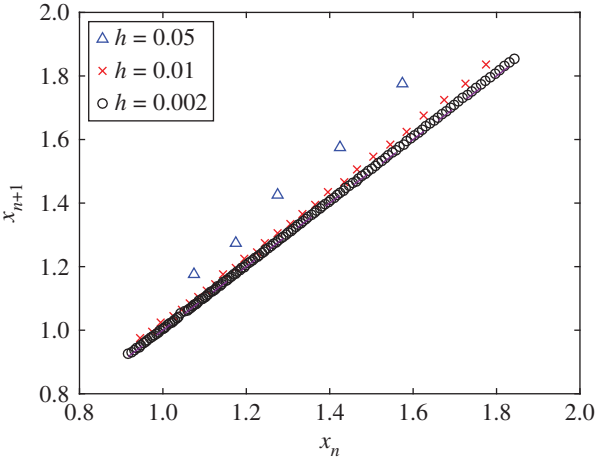

Figure 8. Numerically computed space law for a variety of step sizes on a grid of [0, 10] and time $t = 4$. If a band had more than one grid point, the spike location was computed at the maximal value of d in the band. Plotted for comparison is the line $y = x$. (Online version in colour.)

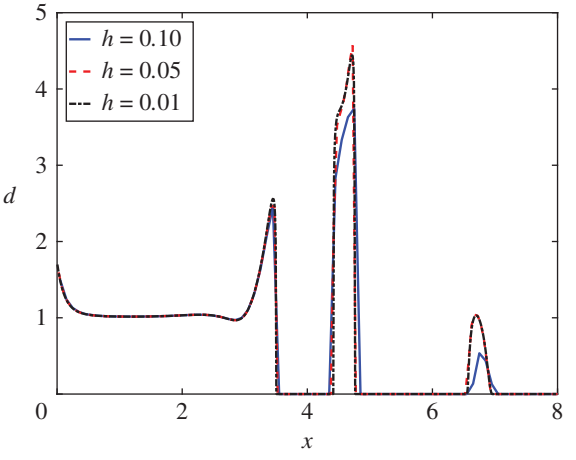

Figure 9. Precipitate numerical solution to (3.17) for a series of step sizes on a grid [0, 10] for $t = 60$ using the smooth precipitate term (5.3) with smoothing parameter $\sigma = 0.5$. The numerical solutions appear to converge as the step size is reduced. (Online version in colour.)

$t = 4$ on a fixed grid [0, 10]. As the step size decreases, the ratio x_{n+1}/x_n approaches a slope of 1, indicating that the $(n + 1)$th spike will overlap the nth spike. This confirms numerically what we showed analytically in (4.11), that a new band forms immediately after the previous one terminates.

The grid scale spike behaviour is due to the presence of a Heaviside-type term, p, given by (3.18). To make the presence of the Heaviside function explicit, (3.18) can be rewritten as

$$p = [AB - \alpha]_+ H([AB - 1]_+ + d); \quad H(z) = \begin{cases} 1, & z > 0, \\ 0, & z \le 0. \end{cases} \tag{5.2}$$

This expression for p can be approximated using a hyperbolic tangent function as

$$p \approx [AB - \alpha]_+ \tanh\left(\frac{[AB - 1]_+ + d}{\sigma}\right), \tag{5.3}$$

where σ is the smoothing parameter. Note that the standard approximation to the Heaviside function is $H(x) \approx \frac{1}{2}[\tanh(x/\sigma) + 1]$, but this takes the value $H(0) = \frac{1}{2}$, whereas we want to strictly enforce $H(0) \approx 0$, as this is an important nucleation threshold. The consequence of the smoothing we have chosen is that our approximation for $H(x) \approx -1$ as $x \to -\infty$; however, because the argument is never negative, we do not need to worry about this negative branch. Figure 9 shows the results of computing d on $[0, 10]$ to $t = 60$ for a variety of step sizes and with the smoothing parameter $\sigma = 0.5$. We note that unlike the grid scale spikes that emerge in the Heaviside model, the location of the secondary bands remains fixed as the step size is reduced and the values of d converge. Unlike the Heaviside model, all of the secondary bands are multiple grid points in size.

6. Conclusion

We set out to establish an asymptotic basis for the approximations used by Keller & Rubinow [10] in their analysis of Ostwald's supersaturation theory for the formation of Liesegang rings. Despite intense effort, we have been unable to find such a basis. Instead, we have shown that in a limit where the diffusivity of $Cr_2O_7^{2-}$ is much less than that of Ag^+, a successful asymptotic solution can be obtained, and we have verified this solution numerically. We also showed that the first precipitation front will terminate, and this is followed by a sequence of subsequent nucleation bands, but that these 'bands' occur as sharp spikes whose width is controlled by, and equal to, the step size used in the numerical computation.

The cause of this ill-posedness lies in the discontinuity in the prescription of the crystal growth rate, but in our discussion of the mechanics of nucleation, we found this discontinuity to be physically appropriate. We also found that if the growth rate function is smoothed, then the secondary bands are of finite width, and the model is well posed. What this suggests is that the ill-posedness of the Keller–Rubinow model is due to the omission of a describing equation for a switching variable, which enables the discontinuity in the growth rate by means of a hysteretic switch between two steady states. While we postpone validation of this concept to a succeeding paper, we suggest here that the switching variable can be taken to be the fractional area coverage $f \in [0, 1]$ of precipitate on nucleating impurities. Thus, $f = 0$ corresponds to $d = 0$ and $f = 1$ to $d > 0$; it is the finite time relaxation of f between these two values which will enable the resolution of the ill-posedness of the Keller–Rubinow model.

Data accessibility. The paper contains no additional data.

Authors' contributions. A.C.F. devised the project and wrote the paper. J.M.D. and I.R.M. constructed and solved the numerical model. All authors performed the literature review, and contributed to the analytic and numerical work. All authors worked on the final text.

Competing interests. We have no competing interests.

Funding. This publication has emanated from research conducted with the financial support of Science Foundation Ireland under grant nos. SFI/12/IA/1683 and SFI/13/IA/1923.

Acknowledgements. We thank Richard Katz of Oxford University, with whose collaboration the experimental work was done.

References

1. Liesegang RE. 1896 Über einige Eigenschaften von Gallerten. *Naturwiss. Wochenschr.* **11**, 353–362.
2. Ostwald W. 1897 Studien über die Bildung und Umwandlung fester Körper. *Zeit. Physik. Chem.* **22**, 289–330. (doi:10.1515/zpch-1897-2233)
3. Ostwald W. 1897 A-Linien von R,E. Liesegang. Referat 83. *Zeit. Physik. Chem.* **23**, 365–384.
4. Morse HW, Peirce GW. 1903 Diffusion and supersaturation in gelatine. *Phys. Rev.* (*Ser.* 1) **17**, 129–150. (doi:10.1103/PhysRevSeriesI.17.129)
5. Wagner C. 1950 Mathematical analysis of the formation of periodic precipitations. *J. Colloid Sci.* **5**, 85–97. (doi:10.1016/0095-8522(50)90008-0)
6. Prager S. 1956 Periodic precipitation. *J. Chem. Phys.* **25**, 279–283. (doi:10.1063/1.1742871)

7. Henisch HK. 1988 *Crystals in gels and Liesegang rings*. Cambridge, UK: Cambridge University Press.
8. Jablczynski K. 1923 La formation rythmique des précipités: les anneaux de Liesegang. *Bull. Soc. Chim. Fr.* **33**, 1592–1597.
9. Stern KH. 1954 The Liesegang phenomenon. *Chem. Rev.* **54**, 79–99. (doi:10.1021/cr60167a003)
10. Keller JB, Rubinow SI. 1981 Recurrent precipitation and Liesegang rings. *J. Chem. Phys* **74**, 5000–5007. (doi:10.1063/1.441752)
11. Flicker M, Ross J. 1974 Mechanism of chemical instability for periodic precipitation. *J. Chem. Phys.* **60**, 3458–3465. (doi:10.1063/1.1681560)
12. Venzl G. 1986 Pattern formation in precipitation processes. II. A postnucleation theory of Liesegang bands. *J. Chem. Phys.* **85**, 2006–2011. (doi:10.1063/1.451144)
13. Müller SC, Ross J. 2003 Spatial structure formation in precipitation reactions. *J. Phys. Chem. A* **107**, 7997–8008. (doi:10.1021/jp030364o)
14. Kai S, Müller SC, Ross J. 1982 Measurements of temporal and spatial sequences of events in periodic precipitation processes. *J. Chem. Phys.* **76**, 1392–1406. (doi:10.1063/1.443131)
15. Volford A, Izsák F, Ripszám M, Lagzi I. 2007 Pattern formation and self-organisation in a simple precipitation system. *Langmuir* **23**, 961–964. (doi:10.1021/la0623432)
16. Mimura M, Ohnishi I, Ueyama D. 2006 A mathematical aspect of Liesegang phenomena in two space dimensions. *Res. Rep. Res. Inst. Math. Sci.* **1499**, 185–201.
17. Venzl G, Ross J. 1982 Comments on pattern formation in precipitation processes. *J. Chem. Phys.* **77**, 1308–1313. (doi:10.1063/1.443953)
18. Falkowitz M, Keller JB. 1988 Precipitation pattern formation. *J. Chem. Phys.* **88**, 416–421. (doi:10.1063/1.454617)
19. Venzl G, Ross J. 1982 Nucleation and colloidal growth in concentration gradients (Liesegang rings). *J. Chem. Phys.* **77**, 1302–1307. (doi:10.1063/1.443952)
20. Polezhaev AA, Müller SC. 1994 Complexity of precipitation patterns: comparison of simulation with experiment. *Chaos* **4**, 631–636. (doi:10.1063/1.166040)
21. Büki A, Kárpáti-Smidróczki É, Zrínyi M. 1995 Computer simulation of regular Liesegang structures. *J. Chem. Phys* **103**, 10 387–10 392. (doi:10.1063/1.469875)
22. Lagzi I. 2003 Simulation of Liesegang patterns: effect of reversible complex formation of precipitate. *J. Phys. Chem. B* **107**, 13 750–13 753. (doi:10.1021/jp036165m)
23. Smoukov SK, Lagzi I, Grzybowski BA. 2011 Independence of primary and secondary structures in periodic precipitation patterns. *J. Phys. Chem. Lett.* **2**, 345–349. (doi:10.1021/jz101679t)
24. Zegeling PA, Lagzi I, Izsák F. 2011 Transition of Liesegang precipitation systems: simulations with an adaptive grid PDE method. *Commun. Comput. Phys.* **10**, 867–881. (doi:10.4208/cicp.050510.031210a)
25. Dowty E. 1980 Crystal growth and nucleation theory and the numerical simulation of igneous crystallisation. In *Physics of magmatic processes* (ed. RB Hargraves), pp. 419–485. Princeton, NJ: Princeton University Press.
26. Becker R, Döring W. 1935 Kinetische Behandlung der Keimbildung in übersättigten Dämpfen. *Ann. Phys.* **24**, 719–752. (doi:10.1002/andp.19354160806)
27. Neu JC, Bonilla LL. 2003 Classical kinetic theory of nucleation and coarsening. In *Mathematical modelling for polymer processing* (ed. V Capasso). Mathematics in Industry, vol. 2, pp. 31–58. Berlin, Germany: Springer.
28. Lifshitz IM, Slyozov VV. 1961 The kinetics of precipitation from supersaturated solid solutions. *J. Phys. Chem. Solids* **19**, 35–50. (doi:10.1016/0022-3697(61)90054-3)
29. Dash JG, Rempel AW, Wettlaufer JS. 2006 The physics of premelted ice and its geophysical consequences. *Revs. Mod. Phys.* **78**, 695–741. (doi:10.1103/RevModPhys.78.695)
30. Fiałkowski M, Bitner A, Grzybowski BA. 2005 Wave optics and Liesegang rings. *Phys. Rev. Lett.* **94**, 018303. (doi:10.1103/PhysRevLett.94.018303)
31. Fowler AC. 2011 *Mathematical geoscience*. London, UK: Springer.
32. Abramowitz M, Stegun IA. 1965 *Handbook of mathematical functions*. New York, NY: Dover.
33. Hilhorst D, vanderHout R, Mimura M, Ohnishi I. 2009 A mathematical study of the one-dimensional Keller and Rubinow model for Liesegang bands. *J. Stat. Phys.* **135**, 107–132. (doi:10.1007/s10955-009-9701-9)